

## Electrochemical properties of $\text{Ca}_{1-x}\text{La}_x\text{TiO}_3$ anode materials for solid oxide fuel cells

Jae-Woo Park<sup>a</sup> and Ki-Tae Lee<sup>a,b,\*</sup>

<sup>a</sup>Division of Advanced Materials Engineering, Chonbuk National University Jeonbuk 54896, Korea

<sup>b</sup>Hydrogen and Fuel Cell Research Center, Chonbuk National University, Jeonbuk 54896 Korea

In this study,  $\text{Ca}_{1-x}\text{La}_x\text{TiO}_3$  (CLT,  $x = 0, 0.05, 0.1, 0.15,$  and  $0.2$ ) was characterized as an anode material for solid oxide fuel cells. The single-phase  $\text{Ca}_{1-x}\text{La}_x\text{TiO}_3$  powder was synthesized in a solid-state reaction via calcination at  $1100\text{ }^\circ\text{C}$  in both oxidizing and reducing atmospheres. The total conductivity of  $\text{Ca}_{1-x}\text{La}_x\text{TiO}_3$  synthesized in a reducing atmosphere was higher than that of  $\text{Ca}_{1-x}\text{La}_x\text{TiO}_3$  synthesized in an oxidizing atmosphere at the same composition due to an increase in the amount of  $\text{Ti}^{3+}$  ions related to charge carrier, based on X-ray photoelectron spectroscopy (XPS) analysis. The  $\text{Ca}_{1-x}\text{La}_x\text{TiO}_3$  showed better tolerance to carbon deposition than Ni-YSZ, and the catalytic activity of the  $\text{Ca}_{1-x}\text{La}_x\text{TiO}_3$  synthesized in an oxidizing atmosphere decreased with increasing La content. Of the  $\text{Ca}_{1-x}\text{La}_x\text{TiO}_3$  synthesized in a reducing atmosphere,  $\text{Ca}_{0.85}\text{La}_{0.15}\text{TiO}_3$  showed the best electrochemical performance.

**Key words:** Solid oxide fuel cells, Anode material, Oxide anode, Carbon deposition.

### Introduction

Solid-oxide fuel cells (SOFCs) are alternative energy devices that generate electricity by converting chemical energy into electrical energy. Ni-YSZ is the most commonly used anode material for SOFC [1, 2] because the Ni catalyst provides high catalytic activity for the hydrogen oxidation reaction (HOR) and high electrical conductivity in SOFCs [3, 4]. There are some disadvantages to the use of Ni-YSZ anodes, such as poor redox stability, low tolerance of sulfur, and the agglomeration of nickel during prolonged operation. Carbon deposition becomes particularly challenging when using hydrocarbon fuel [5-7] and can lead to catalyst deactivation, pore filling, loss of cell performance, and impaired durability [8-10].

Perovskite anode materials are well known for their high tolerance to carbon deposition. Cr- and Ti-based perovskite anode materials have also attracted attention due to their chemical stability in both oxidizing and reducing atmospheres at high temperatures; however, these anode materials exhibit low electrical conductivity and low catalytic activity at intermediate temperatures [11-13].

In this study,  $\text{Ca}_{1-x}\text{La}_x\text{TiO}_3$  (CLT) has been selected as an anode material to improve the catalytic activity and electrical conductivity of SOFCs. Both calcination and sintering of the CLT were performed in a reducing atmosphere in order to increase the efficiency of the reaction.

### Experimental Procedure

The CLT anode materials were synthesized via solid-state reaction. Raw materials of  $\text{La}_2\text{O}_3$  (Alfa Aesar, 99.9%),  $\text{CaCO}_3$  (Alfa Aesar, 99.9%), and  $\text{TiO}_2$  (Alfa Aesar, 99.9%) were mixed and calcined at  $1100\text{ }^\circ\text{C}$  for 16 h in air or 5%  $\text{H}_2/\text{Ar}$ . In order to crush the agglomerated particles during the calcination process, the calcined powders were ball-milled again for 24 h. The flowchart of the powder synthesis is shown in Fig. 1, and the nomenclature of each composition is listed in Table 1.

X-ray diffraction was performed (D/MAX-111A, Rigaku, Japan) with  $\text{Cu K}_\alpha$  radiation to confirm the phases. Diffraction patterns were recorded at a scan rate of  $4^\circ/\text{min}$  in the  $2\theta$  range of  $20^\circ$  to  $80^\circ$ . To measure electrical conductivity, bar-type samples were pressed with a uniaxial press with a  $4 \times 20\text{ mm}^2$  stainless die and then with a cold isotactic press (CIP) to decrease the density gradient. The pressed samples were sintered at  $1450\text{ }^\circ\text{C}$  for 16 h in air. The electrical conductivities were measured using a DC 4 probe in a range of  $600\text{--}800\text{ }^\circ\text{C}$  at  $50\text{ }^\circ\text{C}$  intervals in  $\text{H}_2$  atmosphere.

X-ray photoelectron spectroscopy was conducted (AXIS Ultra DLD Kratos, UK) with monochromatic  $\text{Al K}_\alpha$  at a base pressure of  $5.0 \times 10^{-9}$  Torr to analyze the valence state of the titanium ion. Quantitative analysis of the Ti 2p XPS spectra was performed using XPSPEAK software. The binding energies (BE) were referenced to carbon C (1s) at  $284.5\text{ eV}$ .

The carbon deposition rate was evaluated using a thermal gravimetric analyzer (TGA, TA Q600 TA Instruments Ltd., USA). While the samples were exposed to a  $\text{CH}_4$  atmosphere at  $750\text{ }^\circ\text{C}$  for 1 h, the

\*Corresponding author:  
Tel : +82-63-270-2290  
Fax: +82-63-270-2386  
E-mail: ktleee71@jbnu.ac.kr

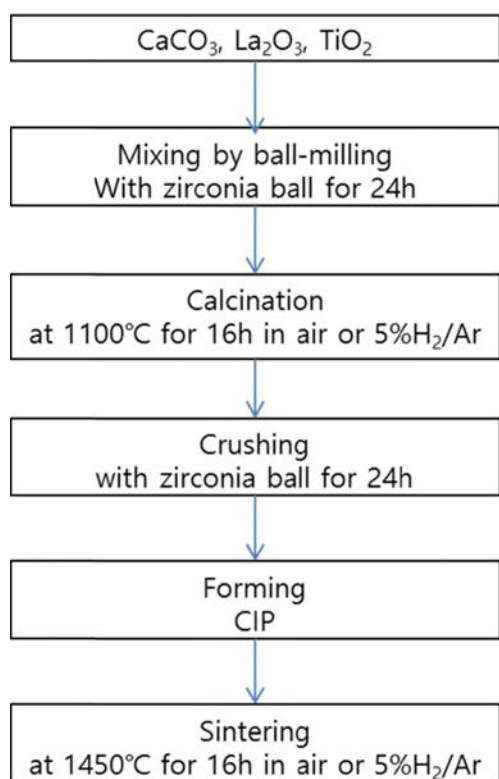


**Fig. 1.** The flowchart for the synthesis of the  $\text{Ca}_{1-x}\text{La}_x\text{TiO}_3$  powders and pellets.

**Table 1.** Nomenclature of the each composition samples.

Nomenclature	Composition
CLT00	$\text{CaTiO}_3$
CLT05	$\text{Ca}_{0.95}\text{La}_{0.05}\text{TiO}_3$
CLT10	$\text{Ca}_{0.9}\text{La}_{0.1}\text{TiO}_3$
CLT15	$\text{Ca}_{0.85}\text{La}_{0.15}\text{TiO}_3$
CLT20	$\text{Ca}_{0.8}\text{La}_{0.2}\text{TiO}_3$

carbon produced from  $\text{CH}_4$  was deposited on the surface of the samples. TGA was carried out from room temperature to  $1000^\circ\text{C}$  at a heating rate of  $10^\circ\text{C}/\text{min}$  in air. The carbon was re-oxidized with oxygen at  $400\text{--}700^\circ\text{C}$  in air. Thus, the amount of deposited carbon can be calculated by analyzing weight loss.

Microstructural characterization of the prepared samples was carried out with a scanning electron microscope (SEM, SN-300 Hitachi, Japan). Electrochemical performance tests were conducted using AC impedance spectroscopy analysis with symmetrical half cells. The electrolyte of the symmetrical half cells was a  $500\text{-}\mu\text{m}$ -thick  $\text{La}_{0.6}\text{Sr}_{0.4}\text{Ga}_{0.8}\text{Mg}_{0.2}\text{O}_3$  (LSGM) pellet. Electrode paste was prepared with CLT powder and polymer binder. The CLT anode layer was screen-printed onto the LSGM pellets and fired at  $1300^\circ\text{C}$  for 2 h. The electrode area of the symmetry cell was  $0.25\text{ cm}^2$ . The AC impedance analysis of the cells was conducted via a galvanopotentiostat (SP150, Biologic SAS, France) with a

frequency response analyzer under an open-circuit at  $800^\circ\text{C}$  in  $\text{H}_2$ . The range of the applied frequency was from 50 mHz to 500 kHz with a voltage amplitude of 25 mV.

## Results and Discussion

X-ray diffraction patterns of the CLT powders are shown in Fig. 2. Synthesized CLT powders in both oxidizing and reducing atmospheres confirmed the formation of perovskite structure without any impurities. The lattice parameters of the CLT powders calculated from X-ray diffraction patterns are shown in Table 2. The lattice parameters of CLT powders synthesized in an oxidizing atmosphere increased with increasing La content, because the ionic radius of  $\text{La}^{3+}$  is larger than that of  $\text{Ca}^{2+}$ . In contrast, there was no regular pattern in the lattice parameters of the CLT powders synthesized in a reducing atmosphere because of the oxygen vacancies that were formed during exposure to the reducing atmosphere. In particular, the CLT20(HH) showed considerably different lattice parameters.

The electrical conductivities of the CLT samples measured in an  $\text{H}_2$  atmosphere are shown in Fig. 3. The CLT samples sintered in an oxidizing atmosphere

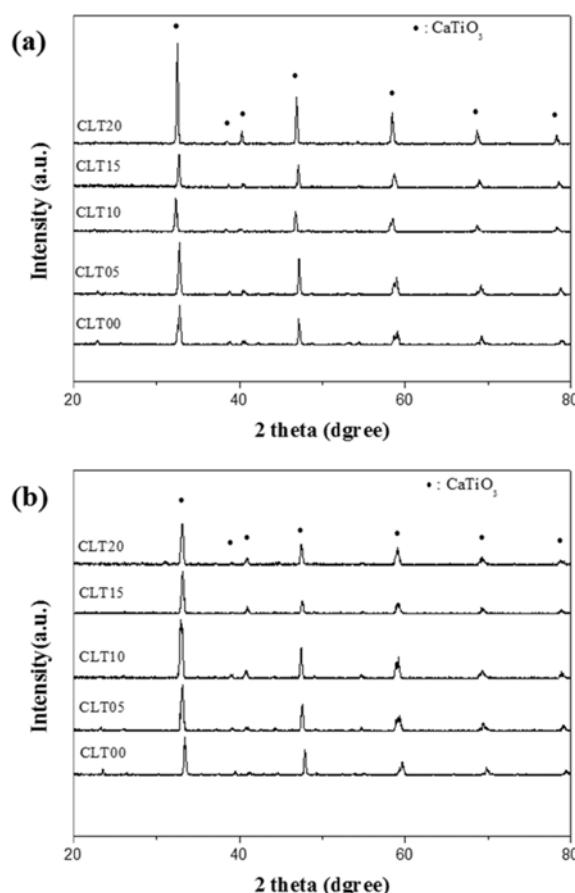


**Fig. 2.** X-ray diffraction patterns of the  $\text{Ca}_{1-x}\text{La}_x\text{TiO}_3$  samples sintered at  $1450^\circ\text{C}$  for 16 h (a) in air and (b) in 5%  $\text{H}_2/\text{Ar}$ .

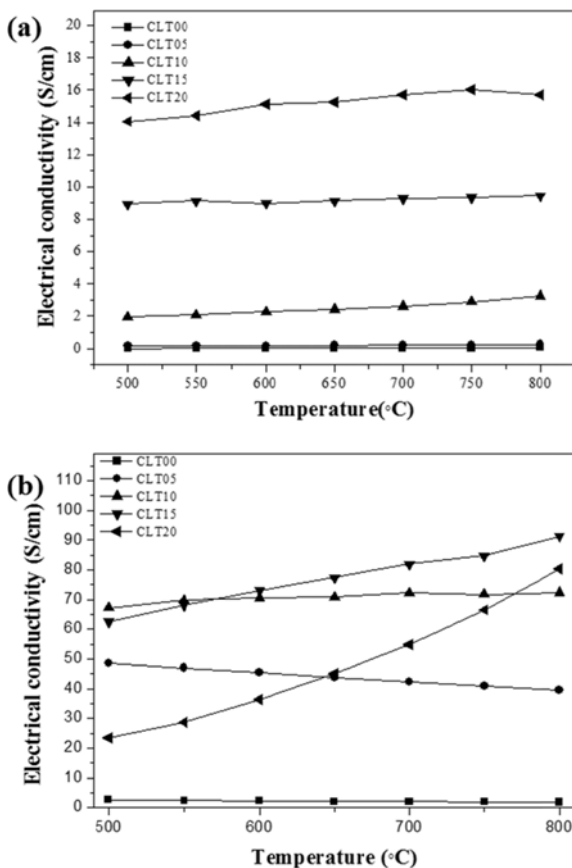
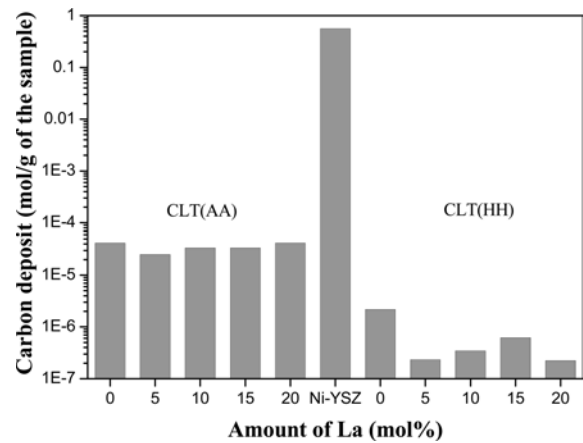
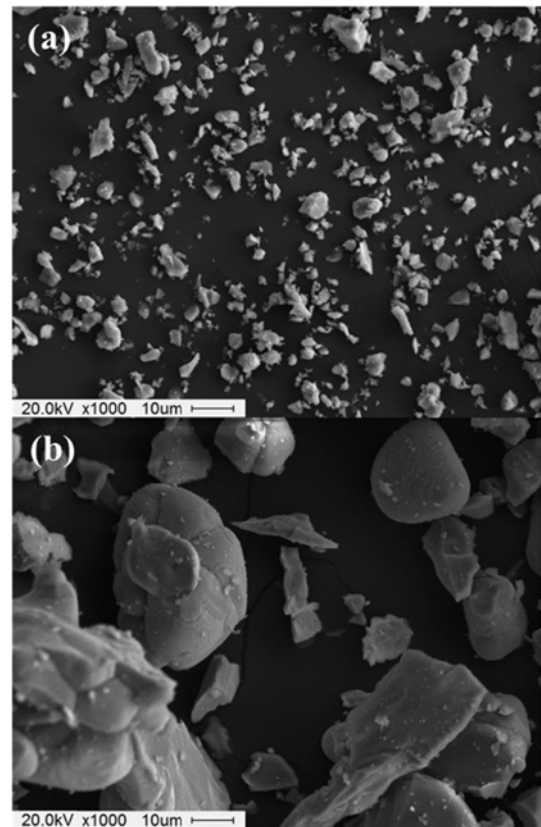
**Table 2.** Calculated lattice parameters of the  $\text{Ca}_{1-x}\text{La}_x\text{TiO}_3$  samples from X-ray diffraction patterns.

Sample	a (Å)	b (Å)	c (Å)
CLT00(AA)	5.421	7.632	5.350
CLT05(AA)	5.349	7.579	5.296
CLT10(AA)	5.393	7.615	5.407
CLT15(AA)	5.429	7.653	5.420
CLT20(AA)	5.434	7.671	5.453
CLT00(HH)	5.224	7.590	5.443
CLT05(HH)	5.433	7.644	5.294
CLT10(HH)	5.424	7.687	5.404
CLT15(HH)	5.425	7.592	5.383
CLT20(HH)	5.682	7.213	5.950

(AA): Calcinated and sintered in air.

(HH): Calcinated and sintered in 5% $\text{H}_2/\text{Ar}$ .**Table 3.** Calculated ratio of  $\text{Ti}^{3+}$  ion from XPS curve fitting.

Sample	$\text{Ti}^{4+}$ (area)	$\text{Ti}^{3+}$ (area)	$\text{Ti}^{3+}$ (%)
CLT00(AA)	26833.6	negligible	–
CLT15(AA)	17610.3	2574.2	7.4
CLT00(HH)	13088.5	1402.9	9.7
CLT05(HH)	11827.7	2160.4	15.4
CLT10(HH)	10317.5	2594.7	20.1
CLT15(HH)	5839.6	3871.5	39.8
CLT20(HH)	8988.1	4494.1	33.3

**Fig. 3.** Electrical conductivities of the  $\text{Ca}_{1-x}\text{La}_x\text{TiO}_3$  samples in a  $\text{H}_2$  atmosphere; the samples were sintered (a) in air and (b) in 5%  $\text{H}_2/\text{Ar}$ .**Fig. 4.** The calculated carbon deposition rate of the  $\text{Ca}_{1-x}\text{La}_x\text{TiO}_3$  anodes after exposure to  $\text{CH}_4$  at 750 °C for 1 h.**Fig. 5.** SEM images of the  $\text{Ca}_{1-x}\text{La}_x\text{TiO}_3$  powders sintered at 1450 °C for 16 h: (a) CLT15(AA) and (b) CLT15(HH).

exhibited increasing electrical conductivity with increasing La content, as well as n-type semi-conducting behavior due to n-type doping. The CLT samples sintered in a reducing atmosphere showed a metallic to semi-conducting transition with La content. While CLT00 and CLT05 showed metallic conduction behavior, the others showed semi-conduction behavior. Also, the electrical conductivity of CLT samples sintered in a reducing atmosphere was significantly higher than that of CLT samples sintered in an oxidizing atmosphere at

the same composition. The maximum electrical conductivity of CLT15(HH) was 91.2 S/cm at 800 °C. Although CLT20(HH) had a higher La content than CLT15(HH), its electrical conductivity was lower due to considerable lattice distortion, which was caused by a large number of  $\text{La}^{3+}$  ions and oxygen vacancies.

The ratio of  $\text{Ti}^{3+}$  ions was calculated from XPS curves and is listed in Table 3. The number of  $\text{Ti}^{3+}$  ions in the CLT samples synthesized in a reducing atmosphere was larger than that of the CLT samples synthesized in an oxidizing atmosphere at the same composition due to charge compensation from the oxygen ion vacancy that occurred in the reducing atmosphere. There was no significant number of  $\text{Ti}^{3+}$  ions in the CLT00(AA) because of the lack of La present in the heat treatment and oxidizing atmosphere. The number of  $\text{Ti}^{3+}$  ions in CLT20(HH) was lower than that of CLT15(HH) due to the relatively higher activation energy and lattice distortion. This charge carrier ratio data is consistent with the trend observed in the electrical conductivity data.

The carbon deposition rate of the CLT samples was compared with that of conventional Ni-YSZ, and the

results are shown in Fig. 4. As expected, CLT samples at all compositions showed significantly lower carbon deposition rates than Ni-YSZ. In addition, the carbon deposition rate of the CLT samples synthesized in a reducing atmosphere was lower compared with that of the CLT samples synthesized in an oxidizing atmosphere. This might be due to the particle size effect related to the activated carbon deposition site.

The morphologies of the CLT powders before experimental carbon deposition are shown in Fig. 5. The particle size of the CLT15(AA) powder was significantly smaller than that of CLT15(HH); thus, CLT15(AA) had a higher surface area compared with CLT15(HH). Carbon deposition occurred on the surface of the catalyst, and these larger surface areas lead to more reaction sites and, ultimately, a higher carbon deposition rate. The cross-sectional images of the CLT symmetry cells are shown in Fig. 6. The thickness of the electrode was measured to be approximately 25 ~ 30  $\mu\text{m}$  for all compositions. The CLT samples sintered in a reducing atmosphere exhibited larger particles than CLT samples sintered in an oxidizing atmosphere.

The AC impedance analysis results for the CLT anodes with a symmetry cell configuration at 800 °C in

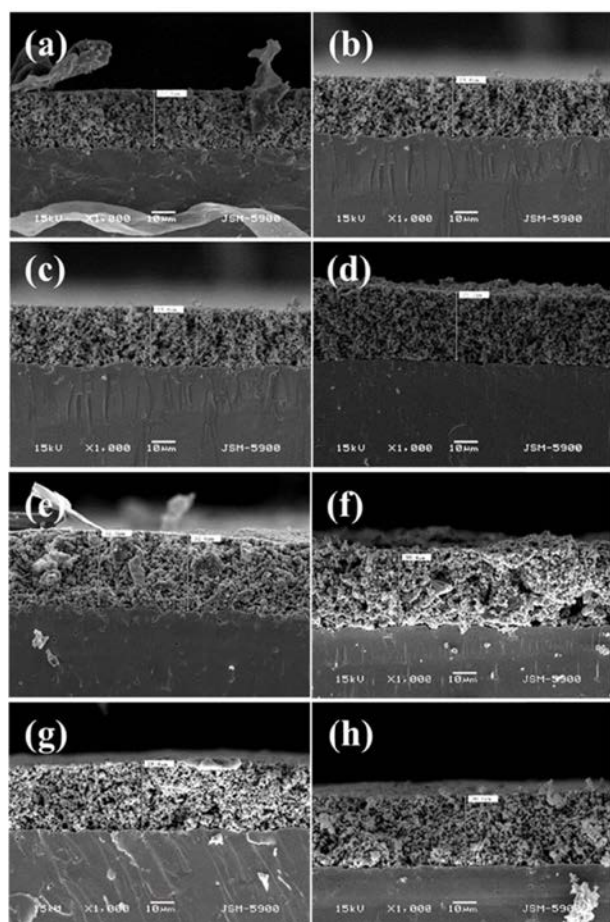


**Fig. 6.** Cross-sectional SEM images of the  $\text{Ca}_{1-x}\text{La}_x\text{TiO}_3$  symmetry cells: (a) CLT00(AA), (b) CLT10(AA), (c) CLT15(AA), (d) CLT20(AA), (e) CLT00(HH), (f) CLT10(HH), (g) CLT15(HH), and (h) CLT20(HH).

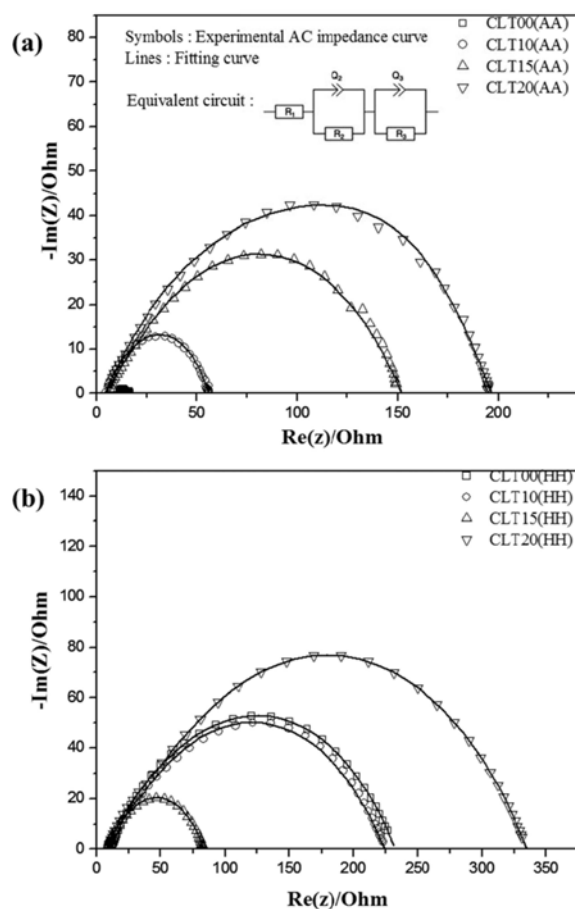


**Fig. 7.** Typical AC impedance spectra of the symmetry cells with  $\text{Ca}_{1-x}\text{La}_x\text{TiO}_3$  sintered (a) in air and (b) in 5%  $\text{H}_2$  / Ar, measured at 800 °C in  $\text{H}_2$ .

H<sub>2</sub> are shown in Fig. 7. The polarization resistance of the CLT synthesized in an oxidizing atmosphere increased with increasing La content. In the CLT synthesized in a reducing atmosphere, the CLT15(HH) showed the lowest polarization resistance due to high electrical conductivity and a large number of oxygen ion vacancies, and the CLT20(HH) showed the highest polarization resistance due to its lattice distortion.

### Conclusions

This study characterized Ca<sub>1-x</sub>La<sub>x</sub>TiO<sub>3</sub> (CLT, x = 0, 0.05, 0.1, 0.15, and 0.2) anode materials for use in SOFC. The CLT powder was synthesized via solid state reaction. The formation of pure perovskite structures was observed in synthesized CLT powders in both oxidizing and reducing atmospheres. While the lattice parameters of the CLT sintered in air increased with the amount of La, the CLT20(HH) showed considerably different lattice parameters due to the lattice distortion caused by the formation of oxygen ion vacancies. The total conductivity of the CLT synthesized in a reducing atmosphere was higher than that of the CLT synthesized in an oxidizing atmosphere at the same composition. The increased total conductivity of the CLT synthesized in a reducing atmosphere was due to an increase in the amount of Ti<sup>3+</sup> ions and was related to the charge carriers, as determined by XPS analysis. The polarization resistance of the CLT synthesized in an oxidizing atmosphere increased with increasing La content. In the case of CLTs synthesized in a reducing atmosphere, CLT15(HH) showed the lowest polarization resistance due to a high electrical conductivity and a large number of oxygen ion vacancies. CLT20(HH) showed the highest polarization resistance due to its lattice distortion. Therefore, CLT15(HH) is considered the optimal composition based on both carbon deposition rate and electrochemical performance.

### Acknowledgments

This work was supported by the New & Renewable Energy Core Technology Program of the Korea Institute of Energy Technology Evaluation and Planning (KETEP) grant and financial resource was provided by the Ministry of Trade, Industry & Energy, Republic of Korea (No. 20143030031430). This work was also supported by the Korea Institute of Energy Technology Evaluation and Planning (KETEP) and the Ministry of Trade, Industry & Energy (MOTIE) of the Republic of Korea (No. 20164030201070).

### References

1. N.Q. Minh, *J. Am. Ceram. Soc.* 76 (1993) 563.
2. S.C. Singhal, *Solid State Ionics* 135 (2000) 305.
3. A. Atkinson, S. Barnett, R.J. Gorte, J.T.S. Irvine, A.J. McEvoy, M. Mogensen, S.C. Singhal, J. Vohs, *Nature Materials* 3 (2004) 17.
4. W.Z. Zhu, S.C. Deevi, *Materials Science and Engineering A* 362 (2003) 228.
5. K. Girona, J. Laurencin, J. Fouletier, F. Lefebvre-Joud, *J. Power Sources* 210 (2012) 381.
6. K.T. Chuang, J. Luo, A.R. Sanger, *Chem. Ind. Chem. Eng. Q.* 14 (2008) 69.
7. J.H. Koh, Y.S. Yoo, J.W. Park, H.C. Lim, *Solid State Ionics* 149 (2002) 157.
8. M.H. Pihlatie, A. Kaiser, M. Mogensen, M. Chen, *Solid State Ionics* 189 (2011) 82.
9. M. Pihlatie, A. Kaiser, M. Mogensen, *Solid State Ionics* 180 (2009) 1100.
10. H. He, J. M. Hill, *Applied Catalysis A: General* 317 (2007) 284.
11. M. Gong, X. Liu, J. Trembly, C. Johnson, *Journal of Power Sources* 1668 (2007) 289.
12. A. Kulkarni, F.T. Ciacchi, S. Giddey, C. Munnings, S.P.S. Badwal, J.A. Kimpton, D. Fini, *International Journal of Hydrogen Energy* 37 (2012) 19092.
13. C. Suna, U. Stimming, *Journal of Power Sources* 171 (2007) 247.